8. Data Report: Electron Microprobe Investigation of Primary Minerals in Basalts from the West Philippine Sea Basin (Ocean Drilling Program Leg 195, Site 1201)[1]

Massimo D'Antonio[2] and Mette B. Kristensen[3]

ABSTRACT

The basement cored at Site 1201 (west Philippine Basin) during Ocean Drilling Program Leg 195 consists of a 91-m-thick sequence of basalts, mostly pillow lavas and perhaps one sheet lava flow, with a few intercalations of hyaloclastite and interpillow sedimentary material. Hydrothermal alteration pervasively affected the basalt sequence, giving rise to a variety of secondary minerals such as K-Fe-Mg-clay minerals, oxyhydroxides and clay minerals mixtures, natrolite group zeolites, analcite, alkali feldspar, and carbonate. The primary minerals of pillow and sheet basalts that survived the intense hydrothermal alteration were investigated by electron microprobe with the aim of characterizing their chemical composition and variability. The primary minerals are mostly plagioclase, ranging in composition from bytownite through labradorite to andesine, chromian-magnesian-diopside, and spinels, both Ti magnetite (partially maghemitized) and chromian spinel. Overall, the chemical features of the primary minerals of Site 1201 basalts correspond to the primitive character of the bulk rocks, suggesting that the parent magma of these basalts was a mafic tholeiitic magma that most likely only suffered limited fractional crystallization and crystallized at high temperatures (slightly below 1200°C) and under increasing $f\mathrm{O}_2$ conditions. The major element composition of clinopyroxene suggests a backarc affinity of the mantle source of Site 1201 basement.

INTRODUCTION

During Ocean Drilling Program Leg 195, 91 m of oceanic crust was cored at Site 1201 from 509 meters below sea floor (mbsf). Site 1201 is situated in the west Philippine Basin at 19°17.8′N, 135°5.9′E, ~100 km west of the present-day submerged and former volcanic arc, Palau-Kyushu Ridge. According to magnetic lineation interpretation (Hilde and Lee, 1984), the basement at Site 1201 is ~49 m.y. old, although this has not been confirmed by paleontological evidence (Shipboard Scientific Party, 2002), and formed during the initial northeast-southwest rifting along the Central Basin Spreading Center. The volcanic basement was subsequently covered by marine sedimentation, first by 2.5 m of red claystone in the late Eocene (>34.3 Ma) (Shipboard Scientific Party, 2002) and second by ~450 m of turbidity current–derived sandstone, silty claystone, breccia, and claystone (53–509 mbsf) from the late Eocene until the early Oligocene (>34.3–30 Ma). These turbidites consist of detrital volcaniclastic material from the Palau-Kyushu Ridge and clasts derived from surrounding carbonate reefs. The turbidite sequence evolved from low-energy turbidite currents in the lower part to high-energy turbidite currents in the upper part. Subsidence of the Palau-Kyushu Ridge eventually brought the turbidite deposition to an end (Shipboard Scientific Party, 2002). Between the late Oligocene and early Pliocene, pelagic sedimentation resumed with emplacement of ~53 m of clays, cherts, and interbedded sandstones and silty claystones (Shipboard Scientific Party, 2002). Pervasive hydrothermal alteration, mainly in an open circulation regime (D'Antonio and Kristensen, 2004), has affected both the pillow and sheet lavas and the hyaloclastite breccia cored at Site 1201, although with decreasing intensity downhole (Shipboard Scientific Party, 2002).

This study presents the results of a mineral chemistry investigation using electron microprobe analysis (EMPA) techniques with the aim of determining the chemical composition and variability of the primary mineral phases of Site 1201 basaltic pillow and sheet lavas. These results were used to infer the chemical composition and differentiation history of the parent magma in order to describe the basement from a petrological point of view.

SAMPLES AND ANALYTICAL TECHNIQUES

Sample Description

Recovery within the 91.4 m cored into the volcanic basement at Site 1201 was ~32%, with exceptionally good recovery within the upper 35 m (>55% recovery). The cored basement consisted of basaltic pillow lava with preserved chilled margins, perhaps one sheet lava flow unit in the lower part, and hyaloclastite fragments mostly in the upper part. Throughout the recovered sequence, chilled glassy pillow margin rims, pillow interiors, hyaloclastite fragments, and interpillow sedimentary material were sampled for shipboard preparation of the thin sections used in this petrographic and chemical study of primary mineral phases.

The cored basement is composed of generally fine grained, sparsely phyric to aphyric basalt. The phenocrysts and microphenocrysts mainly consist of altered plagioclase, although rare olivine pseudomorphs, recognizable by their characteristic rhombic dipyramidal

habit, also appear; clinopyroxene crystals are confined to the groundmass. The hydrothermal alteration decreases significantly in the lowermost cores and is greatest in the upper cores, closest to the pelagic clay contact. Thus, the upper cores have a "rosette" texture due to devitrified glassy groundmass, whereas the interval in the lower part of the core from ~588 to 590 mbsf, presumed to be a sheet lava unit (D'Antonio and Kristensen, 2004), has a more microcrystalline groundmass. Within this unit the grain size is slightly coarser, the alteration is markedly lower (<30 vol%), and no pillow rims are observed; however, pillow rims occur in the same core immediately beneath the sheet lava unit.

Vesicles are present throughout the core but vary in abundance. Abundance is greatest in the upper part of the core and close to chilled pillow margins, where vesicles are seen to coalesce and form outward radiating patterns. Secondary mineral phases such as clay minerals, zeolites, and, less commonly, carbonate occupy vesicles partially or completely. Several millimeter-thick veins are frequent in the upper cores and are often filled by reddish brown interpillow sedimentary material and palagonitized, green, angular glass shards. In the lower cores, veins are generally thinner with clay mineral linings and zeolite or carbonate fillings. A late-stage precipitation of carbonate overprinting earlier clay mineral deposition within veins is often observed. Columnar jointing thermal contraction fractures are observed in two cores, Sections 195-1201D-49R-1 (541.3 mbsf) and 53R-1 (570.3 mbsf), and these fractures also contain a carbonate precipitate.

Hyaloclastite samples primarily found in the upper cores are composed of interpillow sedimentary material (red clays containing fairly deep marine bioclasts, particularly radiolarians) (Shipboard Scientific Party, 2002) and completely palagonitized angular glass shards several millimeters long. Within the shards, colloidal clays and zeolites have replaced the original glass.

Results from major and trace element geochemistry (Shipboard Scientific Party, 2002) allow the basement rocks of Site 1201 to be classified as tholeiitic basalt. Relatively high and variable MgO (8.9–5.8 wt%), Cr (460–324 ppm), and Ni (168–71 ppm) contents, and Mg# (= atomic $100 \times Mg^{2+}/[Mg^{2+} + Fe^{2+}]$; 68%–55%) characterize the basalts; thus, they vary from primitive to moderately fractionated. However, because most samples are highly altered and also revealed by their high loss on ignition (LOI) (0.9–6.6 wt%) (Shipboard Scientific Party, 2002), and because of the mobility of Mg in altered basaltic rocks, the MgO content and Mg# parameter do not reliably indicate the degree of chemical evolution of the magma. On the basis of Ti, Zr, and Y relationships, the basalts cored at Site 1201 exhibit geochemical features intermediate between those typical of mid-ocean-ridge basalts (MORB) and island arc tholeiites (IAT) (Shipboard Scientific Party, 2002). This is in good agreement with similar basalts dredged from the Central Basin Spreading Center (Fujioka et al., 1999), thus confirming their backarc origin.

Investigation Methods and Analytical Techniques

A total of 37 thin sections representative of the recovered cores from basement in Hole 1201D (26 pillow interior/sheet lava, 7 pillow margins, and 4 hyaloclastite samples) were studied using a petrographic microscope. The primary and secondary mineral content and the various textures, veins, and vesicles were examined in order to characterize the

petrography of all samples and constrain the downhole hydrothermal alteration pattern (Shipboard Scientific Party, 2002; D'Antonio and Kristensen, 2004). The primary and secondary minerals were distinguished on the basis of their optical characteristics: primary minerals are those typical of tholeiitic basalts (i.e., plagioclase, clinopyroxene, spinels); secondary minerals are those exotic for tholeiitic basalts (i.e., clay minerals, iron oxyhydroxides, zeolites, alkali feldspar, carbonates) and they replace primary minerals and glass and occur as filling of vesicles and veins. The total degree of alteration, calculated as the sum of the modal abundance of all secondary minerals, varies from 20 to 96 vol% in the investigated samples assumed to be pillow interiors, with least alteration found in samples below 580 mbsf. Alteration in pillow rim samples varies between 66 and 97 vol% and, likewise, the lowermost core samples are the least altered (e.g., Fig. F1D).

The sampled rocks are mostly altered, and therefore EMPA of the secondary mineral phases was performed during subsequent postcruise studies (D'Antonio and Kristensen, 2004). During these studies, when preserved primary minerals were encountered they were also analyzed in order to characterize them chemically and constrain the chemical composition of the parental magma. The primary minerals of pillow and sheet basalts from Site 1201 were analyzed by EMPA in 13 carbon-coated, polished thin sections provided by the Ocean Drilling Program (West Coast Repository, Scripps Institution of Oceanography, La Jolla, California, USA). The investigated samples are representative of the main basement units recognized during shipboard investigations (Shipboard Scientific Party, 2002) and are distributed throughout the recovered cores. EMPA was performed using the Cameca Camebax Microbeam of the Centro di Studi per la Geodinamica Alpina (Consiglio Nazionale delle Ricerche, Padova, Italy), equipped with four vertical wave-dispersion X-ray spectrometers and one energy-dispersion X-ray spectrometer. The electron beam voltage and current were set to 15 kV and 10 nA, respectively, the beam was enlarged to a diameter of 5 μm, and the counting times were set to 10 s for both peak and background. Alkalis were measured first in the routine to prevent their loss under the beam. Data were reduced using a correction procedure for atomic number (Z), X-ray absorption (A), and secondary fluorescence (F) effects (ZAF correction procedure). Both natural and synthetic standards were employed to check the precision and accuracy performance of the instrument.

Petrography

Microscope studies of the Site 1201 basalts revealed distinct textures typical of both pillow rim and pillow interior. Where pillow margin fragments were examined, as in Sections 195-1201D-46R-2, 46R-3, and 48R-4, distinct concentric zones were recognized, thought to reflect the fast cooling of the basalt pillows extruded on the ocean floor. These zones are: (1) an outermost glassy zone, the so-called chilled margin, characterized by sparse, dark brown spherulites enclosed within large patches of light yellow palagonitized glass; (2) an intermediate dark brown spherulitic zone, with closely packed spherulites and no interstitial material; (3) an innermost reddish spherulitic zone, where the spherulites are brown reddish in color and the first plagioclase microliths occur; and (4) a more crystalline interior, with mainly spherulitic, intersertal, and subophitic textures. The transition between the first three zones is gradual, and these zones represent the first 1–2 cm of the

F1. Photomicrographs showing the primary minerals of basalts from Site 1201, p. 12.
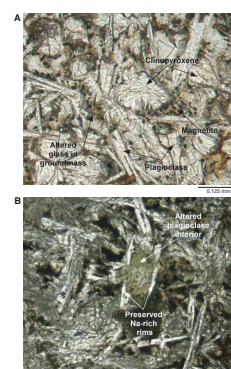
pillow margin rim. No actual holocrystalline pillow cores were observed; however, textures within the pillow interiors in addition to spherulitic (the "rosette" texture visible in hand specimen), intersertal, and subophitic also include hyalopilitic, branching, felty, and intergranular. Some of these textures can also be attributed to the fast cooling of the lava. Additional features confirming this are "swallow-tailed" plagioclase, "featherlike" clinopyroxene, and undulatory extinction of subhedral clinopyroxene crystals.

Plagioclase, olivine, clinopyroxene, and spinels constitute the primary paragenesis observed in Site 1201 basalts. The olivine is always completely replaced by secondary minerals, the plagioclase is commonly preserved only in the lower cores, and the clinopyroxene is the only well-preserved phase throughout the core, although a few cases of recrystallization are observed. The textural relationships among the primary phases suggest early crystallization of plagioclase and olivine followed by clinopyroxene and, eventually, by opaque minerals (Shipboard Scientific Party, 2002). The glass, both in quenched pillow margins and in more crystalline, sheet lava interiors, is always altered to clay minerals and zeolites (Fig. F1A).

Combinations of clay minerals, iron oxyhydroxide, and sometimes analcite or calcium carbonate always completely replace former olivine phenocrysts and microphenocrysts, recognizable by their characteristic rhombic dipyramidal habit. Above 534 mbsf the plagioclase is generally completely replaced by zeolites and alkali feldspar and, more rarely, by clay minerals and/or calcite (D'Antonio and Kristensen, 2004); however, Na-rich rims may be preserved, suggesting an original chemical zoning of the plagioclase (Fig. F1B). Nearly fresh plagioclase is common in basalt from below 532 mbsf in Sections 195-1201D-48R-1 to 55R-2 (Fig. F1D). Clinopyroxene, on the other hand, is always preserved and shows optical features typical of Mg-rich augite (Fig. F1C, F1D). Primary euhedral spinels are magnetite (Fig. F1A, F1D) and, more rarely, deep brown Cr spinel. The abundance of phenocrysts is generally <2% by volume and never exceeds 7% by volume, so rocks range from aphyric through sparsely phyric to moderately phyric (Shipboard Scientific Party, 2002).

RESULTS OF ELECTRON MICROPROBE MEASUREMENTS

Representative EMPA results of primary minerals of Leg 195 Site 1201 basalts are listed in Tables T1, T2, and T3; all the analyses performed are plotted in the diagrams of Figures F2, F3, and F4. The entire analytical set can be provided upon request from the authors.

Plagioclase

The analyses of primary plagioclase phenocrysts, microphenocrysts, and microlites are plotted in the ternary classification diagram Ab-An-Or (Fig. F2). The majority ranges in composition from An_{77} to An_{55}, falling in the fields of bytownite and labradorite; only one individual classifies as andesine (An_{43}) (Table T1). The content of the orthoclase component is always low, generally <0.6 wt%. Overall, the measured compositional range of plagioclase from Site 1201 basement falls within the variation field of plagioclase in basalts from the west Philippine Sea,
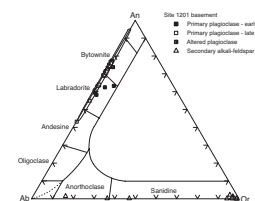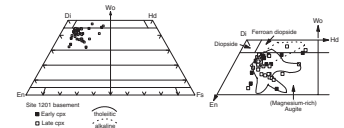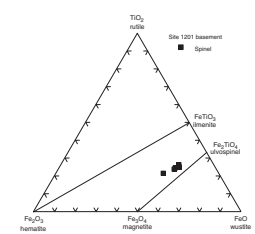
Parece-Vela (Mattey et al., 1981; Zakariadze et al., 1981) and Shikoku (Dick et al., 1980) Basins, as well as the Mariana Trough (Hawkins and Melchior, 1985), shown for comparison in the ternary plot of Figure F2.

Chemical zoning in plagioclase crystals cannot be assessed in most cases because alteration invariably affected the cores; however, when cores are preserved, the zoning is normal and sometimes large core-to-rim variations were detected—for example, from An_{76} to An_{69} (Sample 195-1201D-55R-1 [piece 5R, 103–106 cm] analysis labels 144-122-14 and 144-122-15 in Table T1).

A few plagioclase crystals, petrographically distinguishable by their anomalous greenish color, plot significantly off the main trend in the ternary diagram (Fig. F2) because of a content of the orthoclase component higher than that of primary plagioclase (Or_{1-8} vs. $<Or_{0.5}$) (Table T1). Thus, both optical and chemical characteristics of these individuals indicate that they are incipiently altered. More intensive alteration resulted in some plagioclase crystals being partially or completely replaced by secondary alkali feldspar, variable in composition from nearly pure sanidine ($Or_{99}Ab_1$) to anorthoclase ($Or_{16}Ab_{83}An_1$) (D'Antonio and Kristensen, 2004), shown in the ternary diagram for comparison. In addition, plagioclase replaced by a combination of Na zeolites (natrolite group or analcite), calcite, and smectites was observed (D'Antonio and Kristensen, 2004).

Pyroxene

Pyroxene phenocryst, microphenocryst, and microlite analyses are plotted in the quadrilateral classification diagram Di-Hd-En-Fs (Fig. F3) and classify as chromian-magnesian-augite (Rock, 1990; Yavuz, 2001). Neither orthopyroxene nor pigeonite was detected, as is usual in primitive MORB. The clinopyroxenes display a generally primitive character, as indicated by high Cr_2O_3 contents up to 1.4 wt% and Mg# (= atomic $100 \times Mg^{2+}/[Mg^{2+} + Fe^{2+} + Mn^{2+}]$) of ~85% in the majority of clinopyroxene crystals (Table T2). However, the total range of Mg#s is 88.0%–71.3%. Clinopyroxene crystals also display a short trend of decreasing MgO and CaO and increasing FeO in the quadrilateral classification diagram (Fig. F3), a trend typical of mid-ocean-ridge tholeiite clinopyroxenes (e.g., Hodges and Papike, 1977; Dungan et al., 1978; Mevel et al., 1979; Wood et al., 1979). A few analyses fall off the main trend due to anomalous CaO contents, either higher or lower than other clinopyroxenes with similar Mg#, and/or to Na_2O and TiO_2 contents higher than expected, often resulting in a bad stoichiometry (Table T2). These clinopyroxenes are probably secondary, as they occur in the altered groundmass of some samples (see also Laverne et al., 1995); some of them fall close to, or within, the field of ferroan diopside (Fig. F3).

Spinels

Spinels occur mostly as late-stage, tiny microlites in the groundmass of samples with intersertal, intergranular, and subophitic textures, usually confined within the altered glassy groundmass. The composition is that of Ti magnetite with a high ulvöspinel component (62%–75%) (Table T3; Fig. F4), typical of those from MORB (50%–80%) (Frost and Lindsley, 1991). However, because the analyzed spinels fall distinctly to the left of the magnetite-ulvöspinel join, displaying a ferric iron content higher than fresh magnetite, they are more strictly Ti maghemites (= cation-deficient spinels) (Banerjee, 1991), resulting from oxidation of

Ti magnetite at relatively low temperatures (<300°–400°C). No ilmenite was detected. One microlite of deep brown Cr spinel was detected in Section 195-1201D-54R-1, included in a former olivine grain. It has the composition of a chromian spinel, according to Irvine (1965), with a Cr# (= $100 \times Cr/[Cr + Al]$) of ~55% (Table T3).

DISCUSSION AND CONCLUSIONS

The petrographic evidence that the plagioclase was the liquidus phase (i.e., plagioclase crystals partially enclosed by former olivine crystals) (Shipboard Scientific Party, 2002) is confirmed by the occurrence of individuals relatively rich in the anorthite component (up to An_{77}) (Table T1). However, these are not as rich in Ca as plagioclase of primitive basalts (up to An_{95}) (field enclosing literature data in Fig. F2) from areas close to Site 1201 (i.e., the West Philippine, Parece-Vela, and Shikoku Basins and the Mariana Trough) (Dick et al., 1980; Mattey et al., 1981; Zakariadze et al., 1981; Bougault et al., 1981; Hawkins and Melchior, 1985). This apparent discrepancy can be accounted for because the core of most plagioclase crystals from Site 1201 basalts, which is invariably richer in Ca than the rim, is replaced by secondary minerals.

The overall measured range of plagioclase composition plots very close to the An-Ab join due to low amounts of the orthoclase component (Fig. F2), in agreement with the low K_2O contents in the bulk rocks. The lack of coexisting primary alkali feldspar precludes a precise constraint of the liquidus temperature of the parental magma. However, a rough estimate can be made by applying the plagioclase-liquid geothermometer of Kudo and Weill (1970), refined by Mathez (1973). Assigning the composition of Sample 195-1201D-55R-1, 103–106 cm, as representative of the parental liquid (Shipboard Scientific Party, 2002) and choosing the An-richest plagioclase microlite analyzed in that rock (An_{77}), the geothermometer provides a temperature of 1171°C for P_{H2O} = 0.5 kbar. The measured range of plagioclase compositions is in agreement with the generally primitive character of Site 1201 basalts inferred from bulk rock major and trace element contents (Shipboard Scientific Party, 2002).

The relationships among total Al^{3+}, Si^{4+}, and Ti^{4+} of the analyzed clinopyroxene crystals (Fig. F5) demonstrate that the available Al is more than enough to balance both the Si deficiency in the tetrahedral site (i.e., Al > 2-Si) and the Ti in the octahedral site (i.e., Al:Ti ≥ 6:1). This implies a fundamental role of the Tschermak's components ($CaR^{3+}R^{3+}SiO_6$), particularly the $CaAlAlSiO_6$ component, in the composition of Site 1201 clinopyroxenes and a scarce role of the acmite component ($NaFe^{3+}Si_2O_6$). The latter is testified by the low Na content (<0.03 atoms per formula unit [a.p.f.u.], if only unaltered clinopyroxenes are considered) (Table T2) and the poor Na-Al correlation (not shown). These chemical features, along with the trend of increasing content of Fs at decreasing Wo components and the low Ti (<0.05 a.p.f.u.), are typical of clinopyroxenes from tholeiitic basalts (e.g., Beccaluva et al., 1989). The negative correlation between ($Fe^{2+} + Si^{4+}$) and ($Fe^{3+} + Al^{IV}$) shown in Figure F6, particularly for phenocryst rims and microlites, suggests an increase of fO_2 during the late stages of crystallization of these clinopyroxenes (Vieten, 1980).

The composition of Site 1201 basement clinopyroxenes overlaps with those of tholeiites from other localities in the west Philippine,

F5. Al tot-Si^{4+} and Al tot-Ti^{4+} relationships, p. 17.
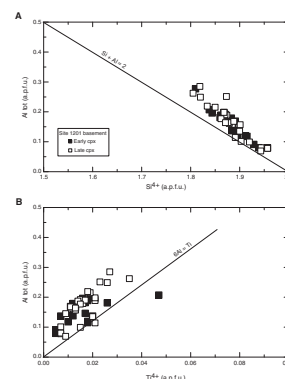
F6. $Fe^{2+}+Si^{4+}-Fe^{3+}+Al^{IV}$ relationships for Site 1201 clinopyroxenes, p. 18.
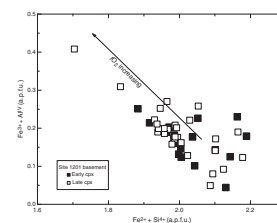
Parece-Vela (Mattey et al., 1981; Zakariadze et al., 1981), and Shikoku (Dick et al., 1980) Basins and the Mariana Trough (Bougault et al., 1981; Hawkins and Melchior, 1985) (Fig. F3); however, some fall in the field of clinopyroxene of alkaline basalts from the Shikoku Basin (Dick et al., 1980), but that is only the effect of their anomalous chemistry, likely a consequence of hydrothermal alteration.

Geothermo-barometric estimates can be made on Site 1201 clinopyroxene, although the lack of coexisting orthopyroxene or pigeonite precludes correct application of two-pyroxene geothermometers such as that formulated by Lindsley (1983). However, projection onto Lindsley's isotherms for P = 1 atm – 5 kbar (Fig. F7) shows that the majority of the analyzed clinopyroxenes fall between the 1100° and 900°C isotherms—although some clinopyroxenes, in particular those with anomalous Na_2O and TiO_2 contents, show equilibration at temperatures as low as 600°C, confirming their secondary origin. In any case, the latter are only rough estimates, as Lindsley's geothermometer can be applied strictly only to high-Ca/low-Ca pyroxene equilibrium pairs. Another geothermometer, formulated specifically for the equilibrium clinopyroxene liquid (Putirka et al., 1996), is more reliable for the studied clinopyroxenes and provides higher temperatures within a narrower range of 1125°–1259°C, with an average of 1195°C (N = 46; STD = 22°C). The altered clinopyroxenes give unreasonably higher temperatures due to the excess of Na and/or Ti. Overall, the temperature estimates for Site 1201 basalts made by means of plagioclase liquid (Kudo and Weill, 1970; Mathez, 1973) and clinopyroxene liquid (Putirka et al., 1996) equilibria are realistic and consistent with the observation that clinopyroxene crystallized later than, or together with, plagioclase and olivine and with the lack of low-Ca pyroxene, which would have crystallized at a temperature of ~1050°C if the basalts were more fractionated (e.g., Demant, 1998). A pressure estimate was performed by means of the geobarometer based on the clinopyroxene liquid equilibrium formulated by Putirka et al. (1996), providing a range of 0–9 kbar with an average of 4.7 kbar (N = 43; STD = 1.9 kbar). The rather large range of pressure can be attributed to the occurrence of both primary clinopyroxene crystals equilibrated at depth before eruption and altered clinopyroxene crystals equilibrated closer to the surface, perhaps during cooling of the lava.
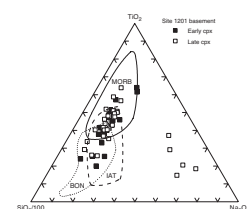
Both temperature and pressure estimates are quite rough and affected by significant uncertainty. This is the result of both the assumptions upon which the geothermometers and geobarometer used are based and of the alteration that affected the minerals. However, these estimates are in sufficiently good agreement with the primitive character of the parent tholeiitic basalt magma of Site 1201 basement.

The composition of all the analyzed Site 1201 clinopyroxenes was plotted into the tectono-magmatic discrimination ternary diagram $SiO_2/100$-TiO_2-Na_2O (Beccaluva et al., 1989) (Fig. F8). This diagram shows that, apart from a few Na-rich secondary individuals, most Site 1201 clinopyroxenes follow a unique trend encompassing both the fields of MORB and IAT. This chemical feature strongly suggests that the Site 1201 basement basalts have a backarc basin affinity.

F7. Portion of the classification diagram Di-Hd-En-Fs for pyroxenes, p. 19.
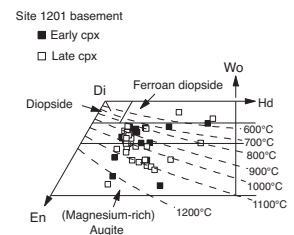
F8. Tectono-magmatic discrimination ternary diagram $SiO_2/100$-TiO_2-Na_2O for clinopyroxene, p. 20.

ACKNOWLEDGMENTS

REFERENCES

Banerjee, S.K., 1991. Magnetic properties of Fe-Ti oxides. *In* Lindsley, D.H. (Ed.), *Oxide Minerals: Petrologic and Magnetic Significance:* Rev. Mineral., 25:107–128.

Beccaluva, L., Macciotta, G., Piccardo, G.B., and Zeda, O., 1989. Clinopyroxene composition of ophiolite basalts as petrogenetic indicators. *Chem. Geol.,* 77:165–182.

Bougault, H., Maury, R.C., El Azzoui, M., Joron, J.L., Cotten, J., and Treuil, M., 1982. Tholeiites, basaltic andesites, and andesites from Leg 60 sites: geochemistry, mineralogy, and low partition coefficient elements. *In* Hussong, D.M., and Uyeda, S., *Init. Repts. DSDP,* 60: Washington (U.S. Govt. Printing Office), 657–666.

D'Antonio, M.D., and Kristensen, M.B., 2004. Hydrothermal alteration of oceanic crust in the West Philippine Sea Basin (Ocean Drilling Program Leg 195, Site 1201): inferences from a mineral chemistry investigation. *Mineral. Petrol.,* 83(1–2):10.1007/s00710-004-0060-6.

Demant, A., 1998. Mineral chemistry of volcanic sequences from Hole 917A, southeast Greenland margin. *In* Saunders, A.D., Larsen, H.C., and Wise, S.W., Jr. (Eds.), *Proc. ODP, Sci. Results,* 152: College Station, TX (Ocean Drilling Program), 403–416.

Dick, H.J.B., Marsh, N.G., and Bullen, T.D., 1980. Abyssal basalts from the Shikoku Basin: their petrology and major element geochemistry. *In* Klein, G. deV., Kobayashi, K., et al., *Init. Repts. DSDP,* 58: Washington (U.S. Govt. Printing Office), 843–872.

Dungan, M.A., Rhodes, J.M., Long, P.E., Blanchard, D.P., Brannon, J.C., and Rodgers, K.V., 1978. The petrology and geochemistry of basalts from Site 396, Legs 45 and 46 of the Deep Sea Drilling Project. *In* Dmitriev, L.V., Heirtzler, J., et al., *Init. Repts. DSDP,* 46: Washington (U.S. Govt. Printing Office), 89–113.

Frost, B.R., and Lindsley, D.H., 1991. Occurrence of iron-titanium oxides in igneous rocks. *In* Lindsley, D.H. (Ed.), *Oxide Minerals: Petrologic and Magnetic Significance.* Mineral. Soc. Am., Rev. Mineral., 25:433–468.

Fujioka, K., Okino, K., Kanamatsu, T., Ohara, Y., Ishizuka, O., Haraguchi, S., and Ishii, T., 1999. Enigmatic extinct spreading center in the West Philippine backarc basin unveiled. *Geology,* 27:1135–1138.

Hawkins, J.W., and Melchior, J.T., 1985. Petrology of Mariana Trough and Lau Basin basalts. *J. Geophys. Res.,* 90:11431–11468.

Hilde, T.W.C., and Lee, C.S., 1984. Origin and evolution of the West Philippine Basin: a new interpretation. *Tectonophysics,* 102:85–104.

Hodges, F.N., and Papike, J.J., 1977. Petrology of basalts, gabbros, and peridotites from DSDP Leg 37. *In* Aumento, F., Melson, W.G., et al., *Init. Repts. DSDP,* 37: Washington, (U.S. Govt. Printing Office), 711–719.

Irvine, T.N., 1965. Chromium spinel as a petrogenetic indicator, Part 1. Theory. *Can. J. Earth Sci.,* 2:648–672.

Kudo, A.M., and Weill, D.F., 1970. An igneous plagioclase thermometer. *Contrib. Mineral. Petrol.,* 25:52–65.

Laverne, C., Vanko, D.A., Tartarotti, P., and Alt, J.C., 1995. Chemistry and geothermometry of secondary minerals from the deep sheeted dike complex, Hole 504B. *In* Erzinger, J., Becker, K., Dick, H.J.B., and Stokking, L.B. (Eds.), *Proc. ODP, Sci. Results,* 137/140: College Station, TX (Ocean Drilling Program), 167–190.

Lindsley, D.H., 1983. Pyroxene thermometry. *Am. Mineral.,* 68:477–493.

Mathez, E.A., 1973. Refinement of the Kudo-Weill plagioclase thermometer and its application to basaltic rocks. *Contrib. Mineral. Petrol.,* 41:61–72.

Mattey, D.P., Marsh, N.G., and Tarney, J., 1981. The geochemistry, mineralogy, and petrology of basalts from the West Philippine and Parece Vela basins and from the Palau-Kyushu and West Mariana ridges, Deep Sea Drilling Project Leg 59. *In* Kroenke, L., Scott, R., et al., *Init. Repts. DSDP,* 59: Washington (U.S. Govt. Printing Office), 753–800.

Mevel, C., Ohnenstetter, D., and Ohnenstetter, M., 1979. Mineralogy and petrography of Leg 46 basalts. *In* Dmitriev, L., Heirtzler, J., et al., *Init. Repts. DSDP,* 46: Washington (U.S. Govt. Printing Office), 151–164.

Putirka, K., Johnson, M., Kinzler, R., Longhi, J., and Walker, D., 1996. Thermobarometry of mafic igneous rocks based on clinopyroxene-liquid equilibria, 0–30 kbar. *Contrib. Mineral. Petrol.,* 123:92–108.

Rock, N.M.S., 1990. The International Mineralogical Association (IMA/CNMMN) pyroxene nomenclature scheme: computerization and its consequences. *Mineral. Petrol.,* 43:99–119.

Shipboard Scientific Party, 2002. Site 1201. *In* Salisbury, M.H., Shinohara, M., Richter, C., et al., *Proc. ODP, Init. Repts.,* 195 [Online]. Available from World Wide Web: http://www-odp.tamu.edu/publications/195_IR/chap_04/chap_04.htm.   [Cited 2002-07-12]

Vieten, K., 1980. The minerals of the volcanic rock association of the Siebengebirge, 1. Clinopyroxenes, and 2. Variation of chemical composition of Ca-rich clinopyroxenes (salites) in the course of crystallization. *Neues Jahrb. Mineral., Abh.,* 140:54–88.

Wood, D.A., Varet, J., Bougaut, H., Corre, O., Joron, J.-L., Treuil, M., Bizouard, H., Norry, M.J., Hawkesworth, C.J., and Roddick, J.C., 1979. The petrology, geochemistry, and mineralogy of North Atlantic basalts: a discussion based on IPOD Leg 49. *In* Luyendyk, B.P., Cann, J.R., et al., *Init. Repts. DSDP,* 49: Washington (U.S. Govt. Printing Office), 597–655.

Yavuz, F., 2001. PYROX: a computer program for the IMA pyroxene classification and calculation scheme. *Comp. Geosci.,* 27:97–107.

Zakariadze, G.S., Dmitriev, L.V., Sobolev, A.V., and Suschevskaya, N.M., 1981. Petrology of basalts of Holes 447A, 449, and 450, south Philippine Sea transect, Deep Sea Drilling Project Leg 59. *In* Kroenke L., Scott R., et al., *Init. Repts. DSDP,* 59: Washington (U.S. Govt. Printing Office), 669–680.

Figure F1. Photomicrographs showing the primary minerals of basalts from Site 1201. **A.** Microphenocrysts and microlites of plagioclase, clinopyroxene, and magnetite in vesicular, altered basalt (Sample 195-1201D-46R-5, 8–11 cm; plane-polarized light). **B.** Microphenocryst of plagioclase showing the core replaced by green clay minerals and preserved Na-rich rims (Sample 195-1201D-48R-2, 74–76 cm; plane-polarized light). (Continued on next page.)

A

Clinopyroxene

Magnetite

Altered
glass in
groundmass

Plagioclase

0.125 mm

B

Altered
plagioclase
interior

Preserved
Na-rich
rims

0.125 mm
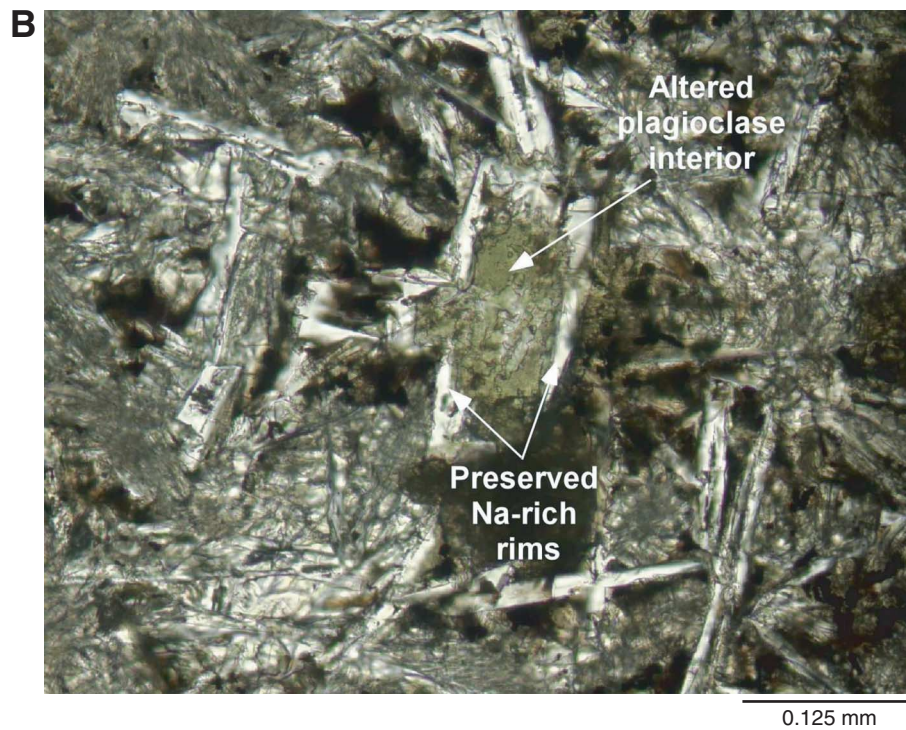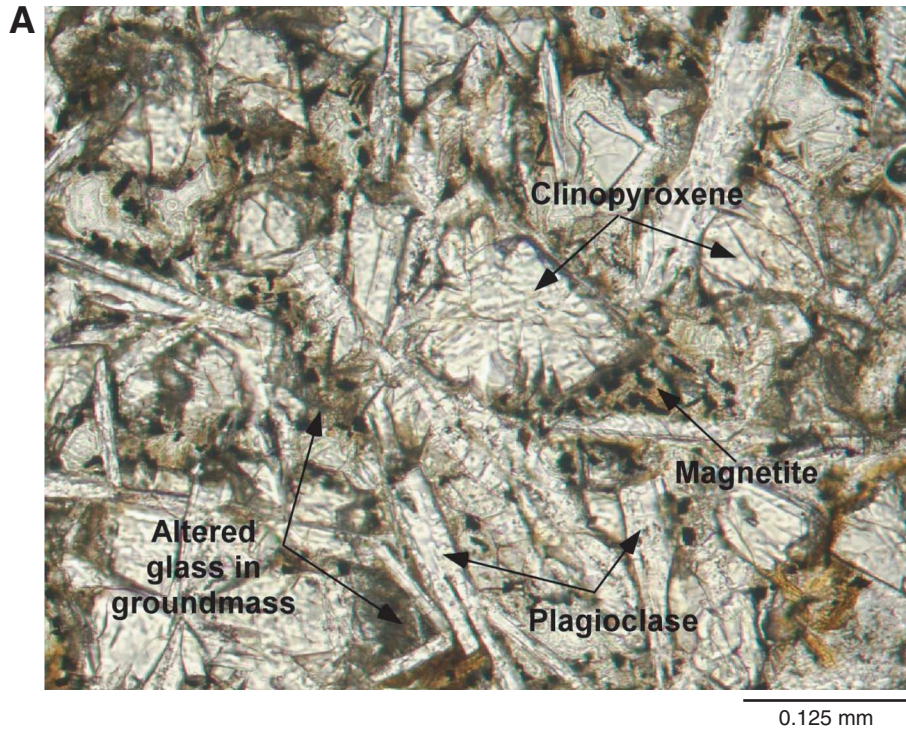
Figure F1 (continued). C. Microlites of clinopyroxene arranged in spherulitic texture within a vesicular, altered glassy groundmass (Sample 195-1201D-46R-5, 8–11 cm; cross-polarized light). **D.** Nearly fresh plagioclase, clinopyroxene, and Ti magnetite in sheet basalt with subophitic texture (Sample 195-1201D-55R-1, 103–106 cm; cross-polarized light).
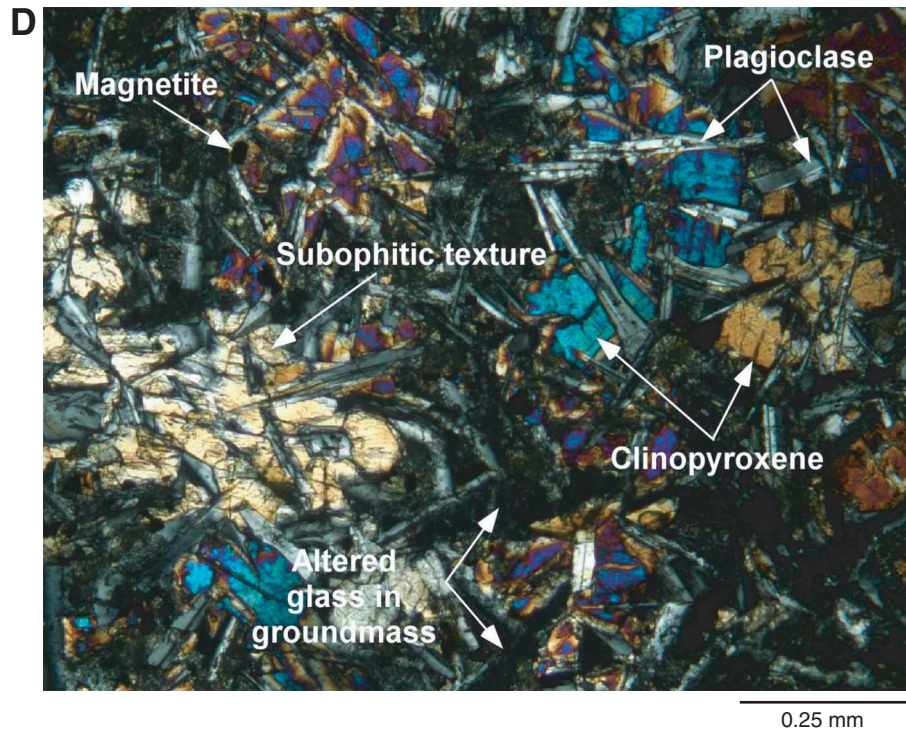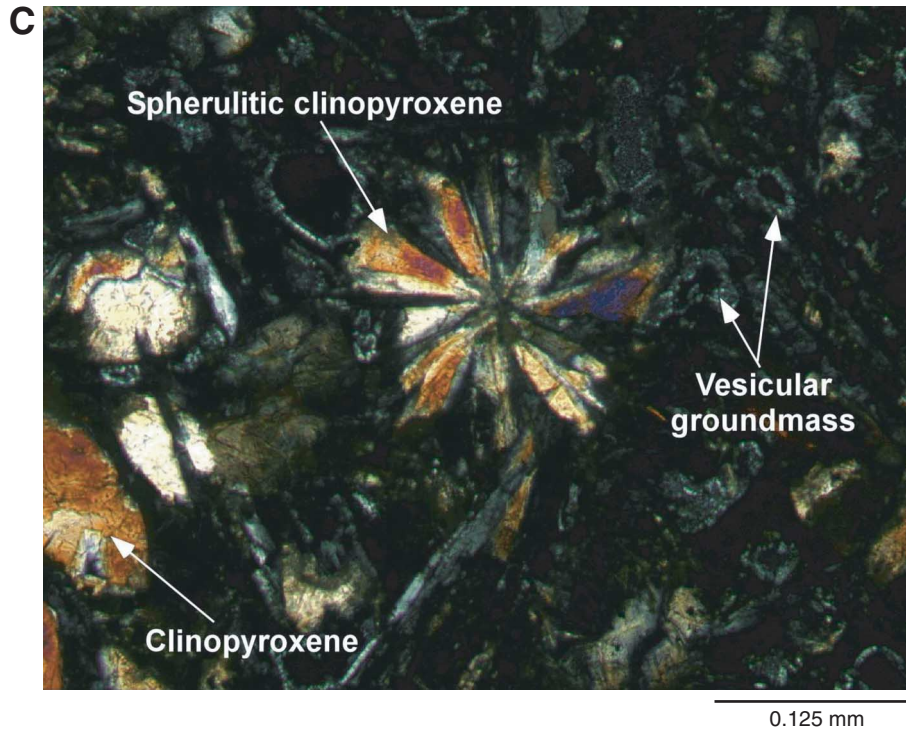
Figure F2. Ternary classification diagram Ab-An-Or for feldspars, showing the chemical variability of primary plagioclase of Site 1201 basalts. Data from Table T1, p. 21. Early = phenocryst cores; late = phenocryst rims, microphenocrysts, and microlites. The enclosed field encompasses the variability range of plagioclase in basalts from the west Philippine, Parece-Vela (Mattey et al., 1981; Zakariadze et al., 1981), and Shikoku (Dick et al., 1980) Basins and the Mariana Trough (Bougault et al., 1981; Hawkins and Melchior, 1985). Data for altered plagioclase and secondary alkali feldspar from D'Antonio and Kristensen (2004).

Figure F3. Classification diagram Di-Hd-En-Fs for pyroxenes (Rock, 1990), showing the chemical variability of clinopyroxenes (cpx) of Site 1201 basalts. Data from Table T2, p. 22. Di = diopside; Hd = hedenbergite; En = enstatite; Fs = ferrosilite; Wo = wollastonite. Early = phenocryst cores; late = phenocryst rims, microphenocrysts, and microlites. The continuous line field encompasses the compositional range of clinopyroxene of tholeiitic basalts from the west Philippine, Parece-Vela (Mattey et al., 1981; Zakariadze et al., 1981), and Shikoku (Dick et al., 1980) Basins and the Mariana Trough (Bougault et al., 1981; Hawkins and Melchior, 1985); the dotted line field represents the compositional range of clinopyroxenes of alkaline basalts from the Shikoku Basin (Dick et al., 1980).
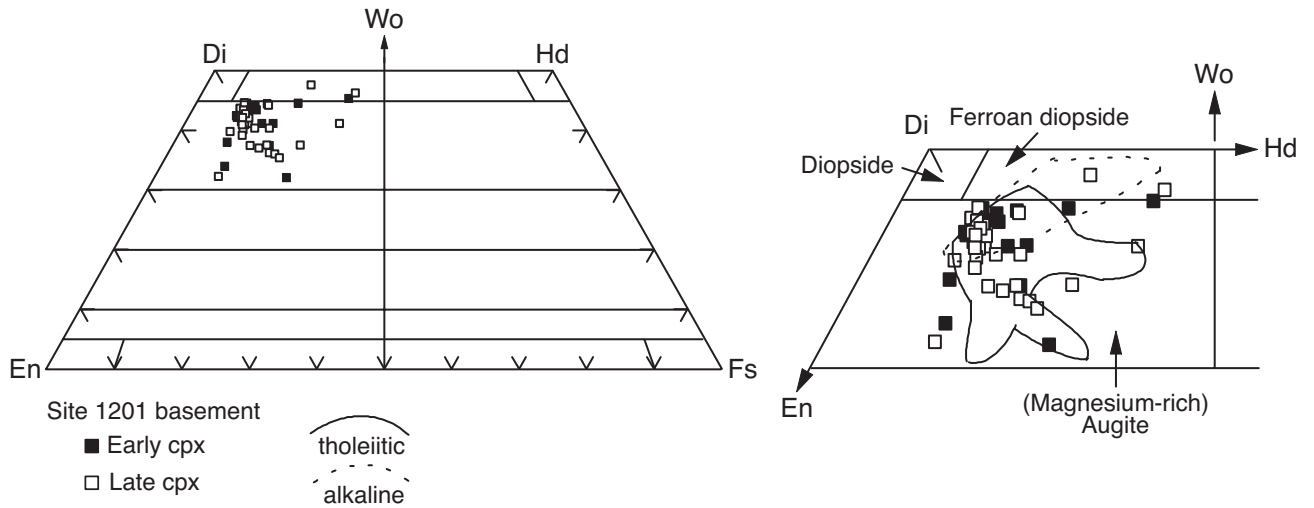
Figure F4. Fe$_2$O$_3$-TiO$_2$-FeO ternary diagram for spinels of Site 1201 basalts. Data from Table T3, p. 24.
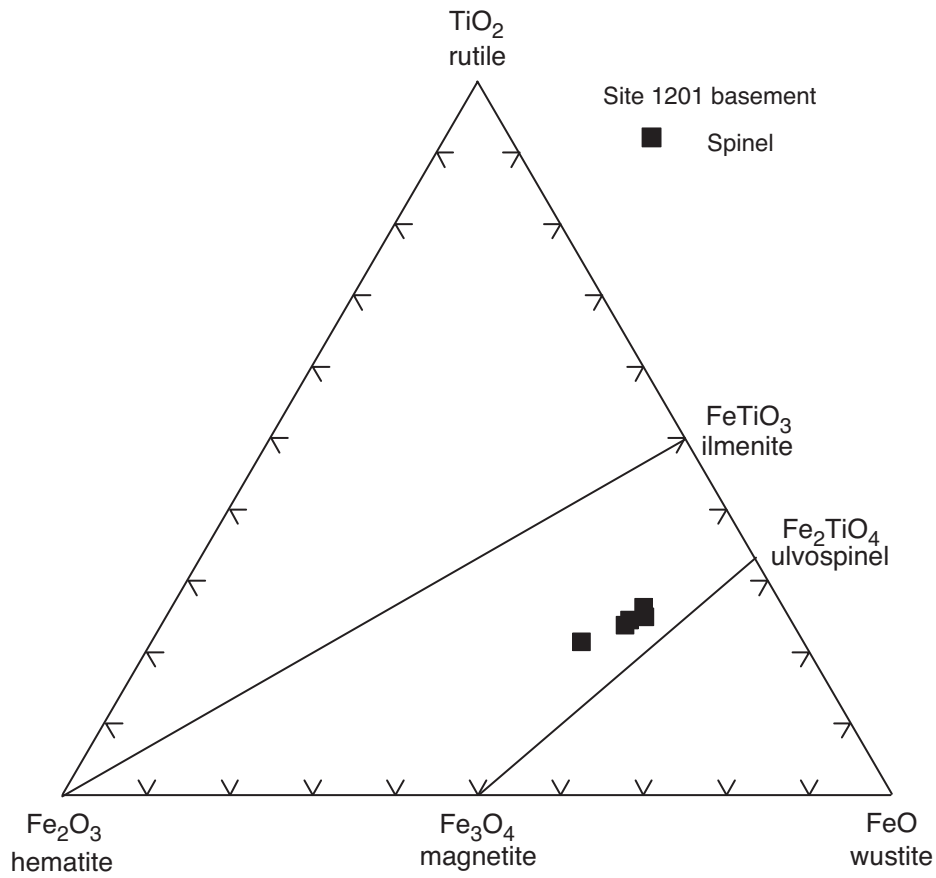
Figure F5. (A) Al tot-Si^{4+} and (B) Al tot-Ti^{4+} relationships for Site 1201 clinopyroxenes (cpx). Data from Table T2, p. 22; the analyses with anomalous chemistry have been excluded. a.p.f.u. = atoms per formula unit.
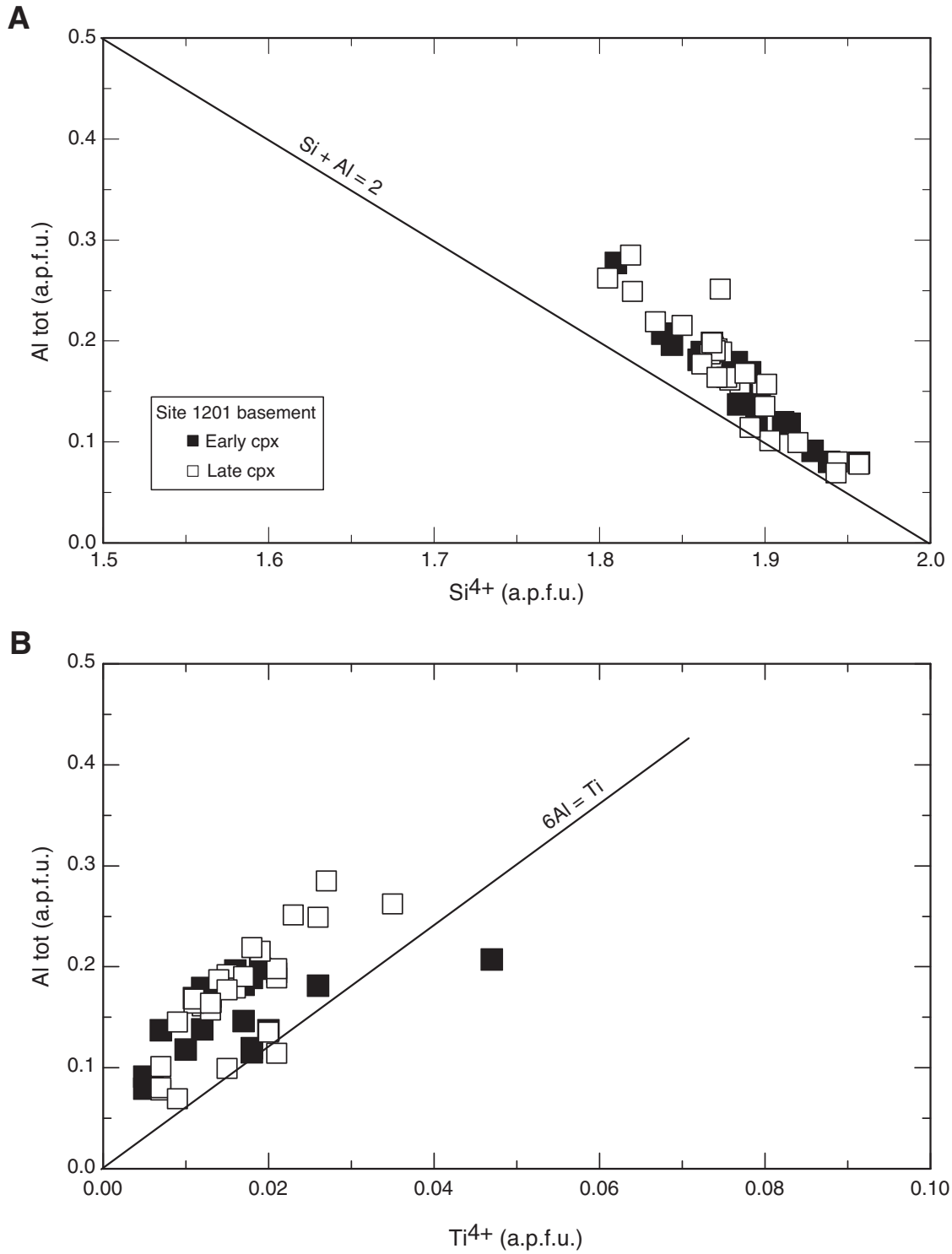
Figure F6. $Fe^{2+}+Si^{4+}$–$Fe^{3+}+Al^{IV}$ relationships for Site 1201 clinopyroxenes (cpx), showing the increasing fO_2 during the late stages of crystallization. Data from Table T2, p. 22; the analyses with anomalous chemistry have been excluded. a.p.f.u. = atoms per formula unit.

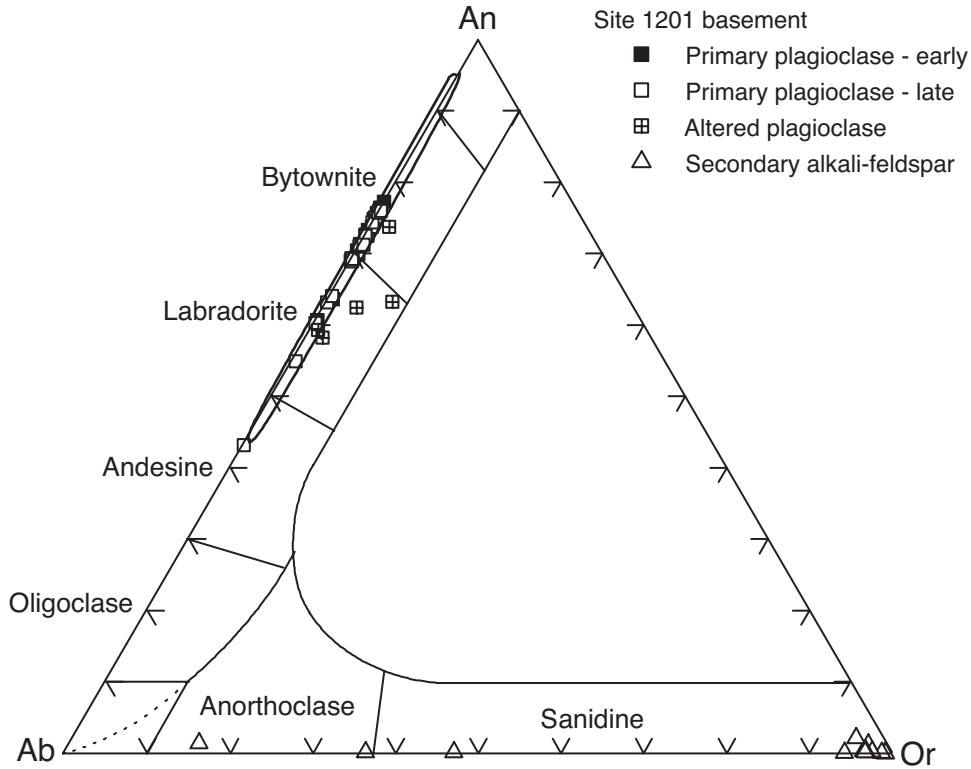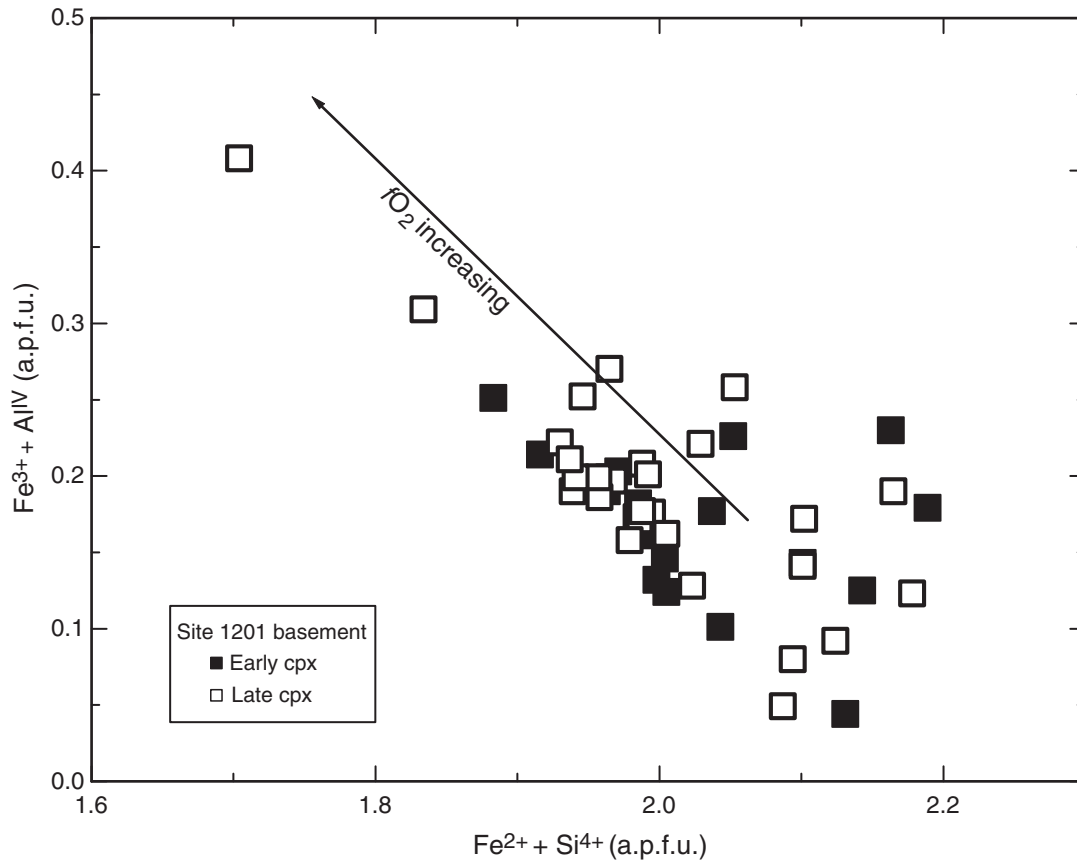**Figure F7.** Portion of the classification diagram Di-Hd-En-Fs for pyroxenes (Rock, 1990), showing the position of clinopyroxenes (cpx) of Site 1201 basalts in relation to the isotherms (*P* = 1 atm – 5 kbar) of Lindsley (1983). Data from Table T2, p. 22. Di = diopside; Hd = hedenbergite; En = enstatite; Fs = ferrosilite; Wo = wollastonite. Early = phenocryst cores; late = phenocryst rims, microphenocrysts, and microlites.

Site 1201 basement

■ Early cpx

□ Late cpx
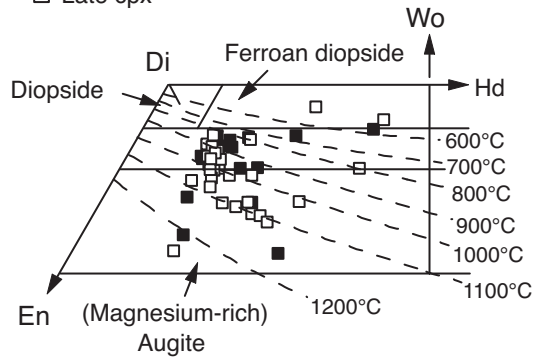
Figure F8. Tectono-magmatic discrimination ternary diagram $SiO_2/100$-TiO_2-Na_2O for clinopyroxene (cpx) (simplified after Beccaluva et al., 1989), showing the chemical variability of clinopyroxene of Site 1201 basalts. Early = phenocryst cores; late = phenocryst rims, microphenocrysts, and microlites. MORB = mid-ocean-ridge basalt; IAT = island-arc tholeiite; BON = boninite.

Table T1. Representative microprobe analyses of plagioclase.

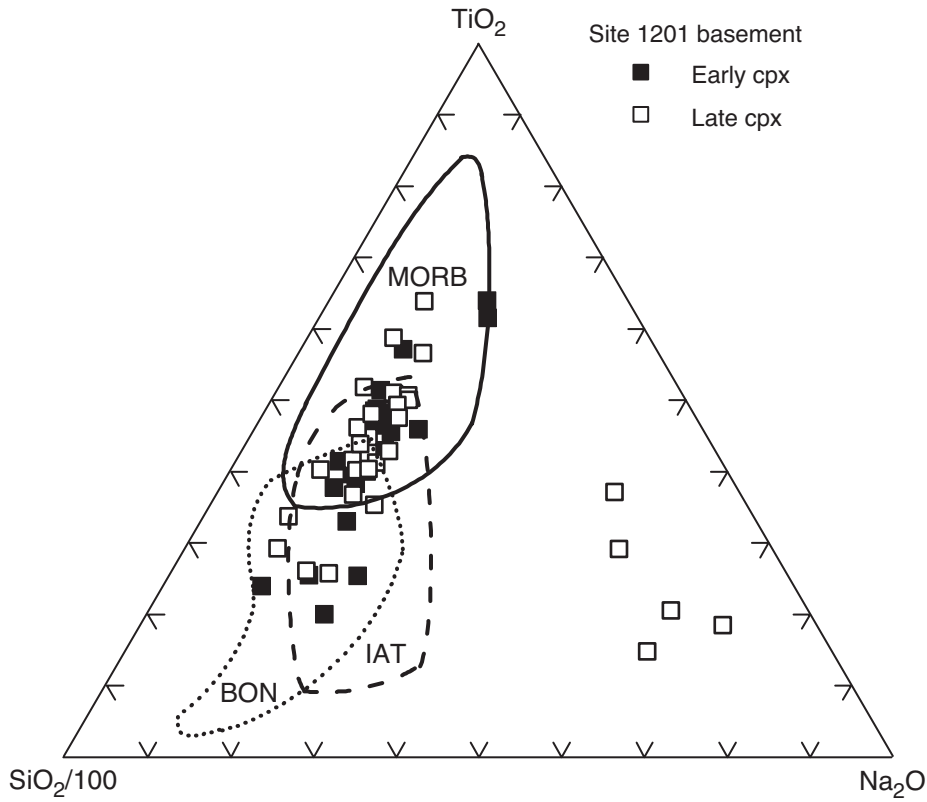| Hole:	195-1201D-											
Core, section, piece, interval (cm):	45R-5 (Piece 1, 103–107)			46R-4 (Piece 6A, 24–27)		48R-2 (Piece 18, 38–41)	48R-2 (Piece 5, 135–138)	49R-1 (Piece 14C, 145–147)	55R-1 (Piece 5R, 103–106)			
Analysis label:	110-3-2	110-3-13	110-10-10	117-22-3	117-29-4	134-101-7	131-51-4	135-112-2	144-122-5	144-122-6	144-122-14	144-122-15
Description:	Micropheno-cryst, rim	Micropheno-cryst, rim	Phenocryst, rim	Altered phenocryst, rim	Altered phenocryst, rim	Microphenocryst, core	Altered phenocryst, rim	Microlite, core	Microlite, core	Microlite, rim	Phenocryst, core	Phenocryst, rim
Major element oxides (wt%):												
SiO_2	54.42	51.27	50.82	54.02	53.13	54.40	53.80	57.72	49.59	50.29	49.57	51.66
TiO_2	0.09	BDL	0.05	0.08	0.07	BDL	0.07	0.11	BDL	0.05	0.07	0.11
Al_2O_3	28.91	30.00	30.30	28.23	28.22	27.39	27.47	26.51	31.24	30.62	31.10	29.63
Fe_2O_3*	1.08	0.77	0.76	1.21	1.01	1.10	0.96	0.56	0.94	0.73	0.70	0.85
MgO	0.24	0.38	0.38	0.21	0.14	0.27	0.59	0.03	0.33	0.33	0.28	0.26
CaO	12.25	14.74	15.16	12.41	11.72	12.71	12.89	9.07	16.29	15.23	15.89	14.24
Na_2O	3.93	3.44	2.95	5.58	4.33	4.54	3.25	6.60	2.66	2.79	2.72	3.49
K_2O	0.03	0.10	0.06	0.09	0.17	0.05	1.37	0.02	BDL	BDL	BDL	BDL
Totals:	100.95	100.70	100.48	101.82	98.79	100.47	100.39	100.61	101.05	100.06	100.33	100.24
Mineralogy (a.f.p.u.):												
Si	9.750	9.311	9.248	9.684	9.745	9.839	9.779	10.304	9.016	9.188	9.059	9.401
Ti	0.012	0.000	0.007	0.011	0.009	0.000	0.010	0.014	0.000	0.007	0.009	0.015
Al	6.105	6.422	6.499	5.964	6.101	5.837	5.885	5.577	6.695	6.594	6.699	6.354
Fe^{3+}	0.146	0.105	0.104	0.163	0.140	0.150	0.131	0.075	0.128	0.101	0.096	0.117
Mg	0.063	0.102	0.102	0.056	0.039	0.071	0.160	0.007	0.091	0.091	0.076	0.070
Ca	2.351	2.868	2.956	2.384	2.302	2.464	2.510	1.734	3.173	2.982	3.112	2.776
Na	1.367	1.213	1.042	1.938	1.541	1.592	1.144	2.284	0.937	0.987	0.966	1.231
K	0.008	0.022	0.013	0.020	0.039	0.012	0.317	0.006	0.000	0.000	0.000	0.000
Totals:	19.801	20.043	19.971	20.220	19.916	19.967	19.935	20.001	20.041	19.950	20.017	19.964
Composition (mol%):												
An	63.11	69.90	73.70	54.90	59.31	60.58	63.19	43.09	77.19	75.07	76.30	69.29
Ab	36.68	29.56	25.98	44.64	39.70	39.14	28.81	56.77	22.81	24.86	23.67	30.71
Or	0.21	0.55	0.32	0.46	1.00	0.28	7.99	0.14	0.00	0.07	0.03	0.00

Notes: Formulas calculated on the basis of 32 oxygens. * = all Fe as Fe_2O_3. BDL = below detection limit, a.p.f.u. = atoms per formula unit, mol% = molar percentage.

Table T2. Representative microprobe analyses of clinopyroxene. (Continued on next page.)

Hole:	195-1201D-						
Core, section, piece, interval (cm):	46R-3 (Piece 10, 99–101)		46R-4 (Piece 6A, 24–27)			47R-2 (Piece 12, 109–111)	
Analysis label:	115-126-4	115-126-5	117-29-5	117-29-6	117-30-2	124-46-1	124-46-2
Description:	Micropheno-cryst, core	Micropheno-cryst, rim	Micropheno-cryst, core	Micropheno-cryst, rim	Altered microlite	Micropheno-cryst, core	Micropheno-cryst, rim
Major element oxides (wt%):							
SiO_2	54.55	51.90	52.82	52.96	51.32	51.95	49.42
TiO_2	0.20	0.41	0.18	0.48	0.34	0.45	0.94
Al_2O_3	1.88	3.92	2.12	3.70	3.44	3.23	5.74
Cr_2O_3	0.52	0.71	0.87	0.27	1.17	0.47	0.16
FeO	5.83	4.49	4.22	5.04	4.33	5.04	6.42
MnO	0.20	0.21	0.14	0.19	0.03	0.00	0.19
MgO	20.51	17.55	18.03	17.42	17.00	17.76	15.51
CaO	17.11	20.64	20.97	21.35	21.81	21.16	21.13
Na_2O	0.10	0.18	0.19	0.18	1.45	0.17	0.17
Totals:	100.90	100.00	99.54	101.59	100.90	100.24	99.67
Fe_2O_3	0.06	1.68	1.95	1.07	9.75	2.79	2.57
FeO	5.77	2.98	2.47	4.07	-4.44	2.54	4.10
Totals:	100.91	100.17	99.74	101.69	101.88	100.52	99.93
Mineralogy (a.f.p.u.):							
Si	1.957	1.888	1.929	1.901	1.837	1.886	1.820
Al^{IV}	0.043	0.112	0.071	0.099	0.145	0.114	0.180
Al^{VI}	0.037	0.056	0.021	0.057	0.000	0.025	0.069
Ti	0.005	0.011	0.005	0.013	0.009	0.012	0.026
Cr	0.015	0.020	0.025	0.008	0.033	0.013	0.005
Fe^{3+}	0.002	0.046	0.054	0.029	0.263	0.076	0.071
Fe^{2+}	0.173	0.091	0.075	0.122	-0.133	0.077	0.126
Mn	0.006	0.006	0.004	0.006	0.001	0.000	0.006
Mg	1.097	0.952	0.982	0.932	0.907	0.961	0.851
Ca	0.658	0.804	0.821	0.821	0.837	0.823	0.834
Na	0.007	0.013	0.014	0.012	0.101	0.012	0.012
Totals:	4.000	4.000	0.000	4.000	4.000	4.000	4.000
Composition (at%):							
Ca	33.97	42.35	42.39	42.98	44.64	42.49	44.14
Mg	56.67	50.13	50.72	48.80	48.40	49.61	45.07
Fe	9.36	7.52	6.89	8.22	6.97	7.91	10.78
Mg#	85.83	86.95	88.05	85.58	87.42	86.25	80.69

Notes: Formulas calculated on the basis of 6 oxygens (software PYROX; Yavuz, 2001). Mg# = $100 \times Mg^{2+}/(Mg^{2+} + Fe^{2+} + Mn^{2+})$. Fe* = $Fe^{3+} + Fe^{2+} + Mn^{2+}$. BDL = below detection limit, a.p.f.u. = atoms per formula unit, at% = atomic percentage.

Table T2 (continued).

Hole:			195-1201D-				
Core, section, piece, interval (cm):	48R-2 (Piece 18, 38-41)	49R-1 (Piece 14C, 145–147)		55R-1 (Piece 5R, 103–106)			
Analysis label:	134-105-1	135-107-5	135-107-6	144-123-7	144-123-8	144-122-9	144-122-10
Description:	Altered microlite	Intergrown with plagioclase	Intergrown with plagioclase	Microlite, core	Microlite, rim	Microlite, core	Microlite, rim
Major element oxides (wt%):							
SiO_2	49.82	49.95	50.47	50.86	51.77	51.71	52.78
TiO_2	1.69	0.66	1.00	0.95	0.72	0.66	0.55
Al_2O_3	4.76	5.07	6.71	4.20	3.13	2.66	2.32
Cr_2O_3	0.09	0.14	0.22	0.58	0.10	BDL	BDL
FeO	9.02	10.12	8.30	6.34	7.86	12.01	9.90
MnO	0.06	0.31	0.17	0.20	0.18	0.46	0.24
MgO	13.72	16.66	16.70	15.74	16.48	17.37	17.35
CaO	21.03	17.16	17.90	21.53	19.75	15.98	18.05
Na_2O	0.56	0.23	0.26	0.20	0.23	0.20	0.17
Totals:	100.75	100.31	101.72	100.61	100.22	101.05	101.36
Fe_2O_3	2.29	3.33	1.50	2.23	1.47	2.66	1.57
FeO	6.96	7.12	6.95	4.33	6.53	9.61	8.49
Totals:	100.98	100.64	101.87	100.84	100.37	101.32	101.52
Mineralogy (a.p.f.u.):							
Si	1.838	1.834	1.819	1.860	1.900	1.895	1.920
Al^{IV}	0.162	0.166	0.181	0.140	0.100	0.105	0.080
Al^{VI}	0.045	0.054	0.104	0.041	0.035	0.010	0.019
Ti	0.047	0.018	0.027	0.026	0.020	0.018	0.015
Cr	0.003	0.004	0.006	0.017	0.003	0.000	0.000
Fe^{3+}	0.064	0.092	0.041	0.061	0.041	0.073	0.043
Fe^{2+}	0.215	0.219	0.209	0.133	0.201	0.295	0.258
Mn	0.002	0.010	0.005	0.006	0.005	0.014	0.007
Mg	0.755	0.912	0.897	0.858	0.902	0.949	0.941
Ca	0.831	0.675	0.691	0.844	0.777	0.627	0.704
Na	0.040	0.016	0.019	0.014	0.016	0.014	0.012
Totals:	4.000	4.000	4.000	4.000	4.000	4.000	4.000
Composition (at%):							
Ca	44.55	35.39	37.48	44.36	40.34	32.03	36.02
Mg	40.44	47.80	48.67	45.12	46.85	48.45	48.17
Fe	15.01	16.80	13.85	10.52	12.81	19.52	15.80
Mg#	72.93	73.99	77.85	81.09	78.53	71.28	75.30

Table T3. Representative microprobe analyses of spinels.

Hole:	195-1201D-			
Core, section, piece, interval (cm):	54R-1 (Piece 4, 41–43)		55R-1 (Piece 5R, 103–106)	
Analysis label:	141-125-1	141-125-2	144-122-12	144-122-17
Description:	Microlite core	Microlite rim	Microlite	Microlite
Major element oxides (wt%):				
SiO_2	0.06	0.06	0.17	0.25
TiO_2	0.52	0.51	19.42	22.89
Al_2O_3	23.11	23.21	1.80	2.35
Cr_2O_3	42.49	41.89	BDL	0.02
FeO	19.36	19.11	68.98	62.90
MnO	0.25	0.12	0.68	0.63
MgO	14.32	14.49	0.43	0.67
CaO	0.12	0.13	0.17	0.16
Totals:	100.23	99.52	91.66	89.87
Usp (mol%)			62.04	75.09
Cr#	55.22	54.77		

Notes: BDL = below detection limit, Usp = ulvöspinel. Cr# = $100 \times Cr/(Cr + Al)$. Mol% = molar percentage.